Helium Bubble Survey of a Parachute-Opening Flowfield Using Computer Graphics Techniques

Paul C. Klimas*
Sandia Laboratories, Albuquerque, N. Mex.
and
David F. Rogers†
U. S. Naval Academy, Annapolis, Md.

Neutrally buoyant helium-filled soap bubbles were used to determine fluid particle pathlines and velocities in the airstream surrounding an 18-in. nominal diameter flat circular parachute model. The bubbles, dynamically indistinguishable from the air that they displaced and highly reflective because of their soap film outer surface, were photographed in two orthogonal planes by high-speed motion picture cameras. Positions of matched bubble pairs from the two views were entered into computer files frame by frame by projecting the films onto a digitizing tablet and using a light pen. This information, along with the film frame rates, was used to time-differentiate the pathlines to produce velocity data. Some 3000 bubble-frame pairs generated velocity plots covering the region near the canopy for times between $T=0$ and steady-state conditions.

I. Introduction

EXPERIMENTAL knowledge of the particle velocities in the flowfields surrounding opening parachutes may be utilized at a number of stages in the design process. The mathematical modeler may incorporate actual locations of separation points and vortex strengths and shedding points in his analytical representation of the device, as well as all of the flowfield data to verify the accuracy of the model. Details of certain localized flow changes due to perturbations in the composition of the canopy-payload-suspension system could improve the understanding of the effects of these changes on system performance. Certain forces also may be inferred from purely kinematic flowfield information. Heinrich[1] and White[2] have shown that assumed canopy inflow velocity profiles can be used to calculate parachute-opening forces.

Although this type of velocity data is advantageous to have, it is generally unavailable. The primary reason for this is that most measuring devices either physically obstruct the flow or opening canopy because of their size (hot-wire anemometers, pressure rakes) or cannot function in areas of high fluid rotation (pressure rakes, smoke) such as are found in wakes or mouth regions. One device, however, which has none of these failings is the helium bubble generator. Pounder[3] in 1956 mapped steady-state flowfields about various wind-tunnel model canopies by injecting neutrally buoyant helium-filled soap bubbles into the stream passing the model and photographing them in a single plane. The neutral buoyancy made the bubbles dynamically indistinguishable from the air that they displaced, and the high-reflectivity soap film outer surface gave a high degree of photographic discrimination. The 1973 extension of this idea by Klimas[4] included certain unsteady flowfield information and eliminated the need to assume a planar flow by making two simultaneous orthogonal photographs. Two major problems arose in this study. The low wind-tunnel speeds (10 fps) required to allow sufficient bubble residence time for photographs to be made caused the horizontally deploying parachute model to have an unacceptable asymmetry until very late in the opening process. As a result, only unsteady data for a nondimensional filling time T (ratio of the time measured from suspension line extension to that from extension to the first attainment of a canopy-projected area equal to that under steady-state conditions) of unity were gathered. Secondly, the vast amounts of data generated dictated that any future study of this type should incorporate a sophisticated computer-based data-processing scheme. The present paper details the changes made to overcome these problems and to develop a much more complete flowfield description.

II. Apparatus

As was its predecessor,[4] the experiment was run in the U.S. Naval Academy 3.5- × 4.5-ft subsonic wind tunnel and used the same parachute and deployment system (Fig. 1). The model was an 18-gore, 18-in. nominal diameter flat circular

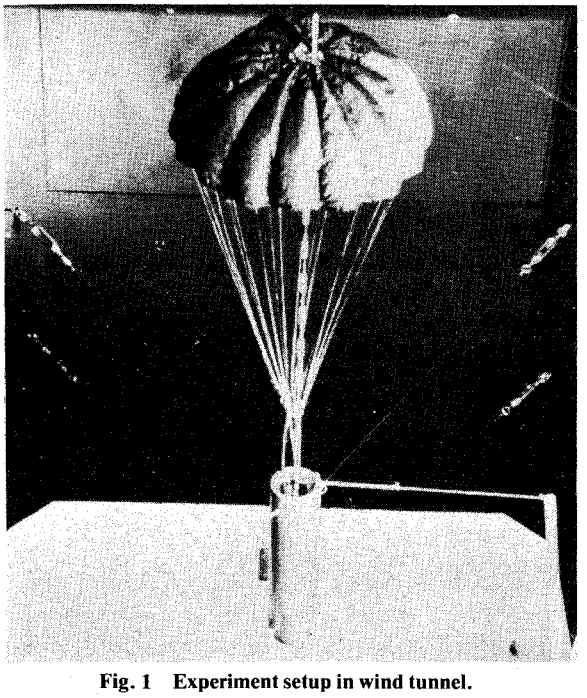

Fig. 1 Experiment setup in wind tunnel.

Presented as Paper 75-1368 at the AIAA 5th Aerodynamic Deceleration Systems Conference, Albuquerque, N. Mex., Nov. 17-19, 1975; submitted Jan. 15, 1976; revision received April 22, 1977.
Index categories: Nonsteady Aerodynamics; Deceleration Systems.

*Member of Technical Staff, Aerodynamics Department. Member AIAA.
†Professor, Aerospace Engineering Department. Member AIAA.

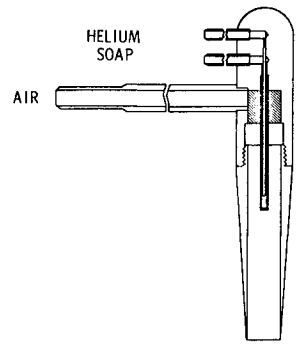

Fig. 2 Cross-sectional schematic of the bubble generator head.

type with a 1.8-in.-diam vent.‡ The canopy was made up of 1.1-oz rip-stop nylon, MIL-C-7020, type I, with a permeability of 114 $ft^3/ft^2/min$. Suspension lines had a length of 18 in. terminating on a 15/16-in.-diam steel ring. The parachute was loosely packed into a 3-diam, 1-ft-long, streamlined aluminum tube. The deployment sequence was initiated by lifting a solenoid-driven packing pin. This allowed a dead-fall weight, attached to the vent ring by a line stretching down the tunnel centerline to the end of the test section, to pull the parachute along a 5-ft-long, 0.25-in.-diam centerline-mounted aluminum rod to a point where the airstream began the inflation. The rod was necessary in order to prevent model coning. In steady operation, the suspension line ring was some 6 in. downstream of the deployment tube.

The helium-filled soap bubbles were formed by a Sage Action, Inc. generating system using a low-speed generating head (Fig. 2). The head may be seen mounted near the left margin of Fig. 1. The manufacturer cites their bubble densities as being within ±2% of the tunnel air value. For maximum bubble definition and minimum reflection, the model and tunnel background were painted flat black. Motion pictures were taken from two orthogonal positions using 16-mm Fastax cameras set to operate at approximately 1700 frames/sec with Eastman XX negative film. Lighting was via five 500-W photoflood lamps evenly spaced along a 4-ft length of the test section inner wall and angled such that both top and side cameras received equal lighting. This lighting was adequate to allow f5.6-8 settings on the camera lenses and a film exposure index of 800 ASA, with the tunnel airspeed set near 100 fps. This tunnel speed gave a ratio of aerodynamic to static forces during the horizontal opening which was two orders of magnitude higher than that of the percursor study and resulted in no notable lack of opening canopy symmetry. The cameras were placed from 9 to 15 ft from the model, depending upon the lenses used.

III. Experiment

With the tunnel speed at 96 fps, the bubble generator was set to produce ⅛-in.-diam bubbles at a rate of approximately 200/sec. This resulted in an average separation distance between individual bubbles of 6 in. or so, usually making positive identification of a given bubble in both side and top views a simple matter. The event time covered an average of approximately 40 msec, resulting in 15 or so bubbles in each run from which information could be obtained. The time interval began with suspension line extension and was twice as long as the time required to attain canopy maximum projected area. The number of frames occupied by each bubble ranged from two or three to 40. Films were made of ten different runs, with the upstream location of the generating head being changed between runs so as to distribute bubbles throughout the entire flowfield. The resulting raw data then were roughly 3000 different bubble-frame points recorded in two orthogonal views as a function of time and occupying the region surrounding the opening canopy.

‡Furnished by W. P. Ludtke, Naval Surface Weapons Center.

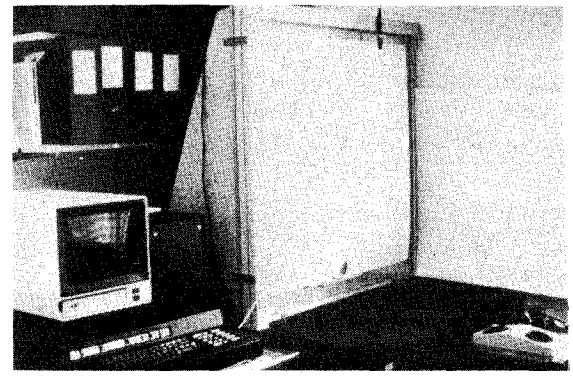

Fig. 3 Bubble location digitizing apparatus.

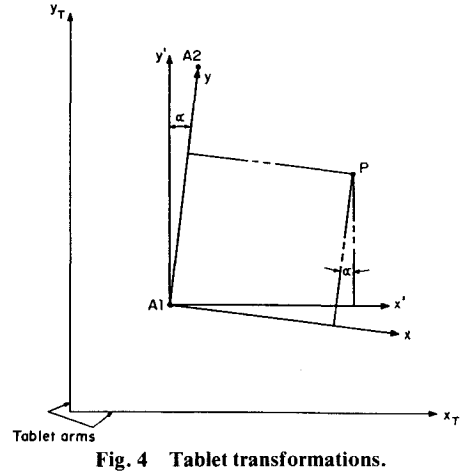

Fig. 4 Tablet transformations.

IV. Data-Reduction Scheme

Overview

The orthogonal films then were time-synchronized and projected frame by frame onto a digitizing tablet. The locations of individual bubbles with associated reference points then were digitized in the two orthogonal views frame by frame. This technique provides a time history of the two-dimensional particle path line of a helium bubble in the two orthogonal views. Use of computer graphics techniques then allows the determination of a three-dimensional particle path line. These particle path lines then are differentiated using finite-difference techniques to yield the Cartesian velocity components. The details of each individual step in the data-reduction scheme are discussed below.

Film Preparation

Each pair of films was handled as a unit. In order to determine a common "zero" time, each film was examined frame by frame to determine that point in time, i.e., the particular frame, at which full suspension line extension occurred. This frame then was considered the zero frame. All subsequent frames were numbered from this frame. The frame rate for each camera was different. Individual frame rates were determined by timing marks superimposed on the film.

Digitization

Each film then was projected frame by frame onto a 36- × 36-in. Science Accessories Corporation (SAC) analog tablet connected to a Conographic-10 storage tube CRT graphics terminal supported by a Honeywell 635 time-sharing computer system (see Fig. 3). Individual bubbles, along with calibration symbols, were digitized in each frame. The digitized results were stored in each frame. The digitized results were stored in a data file for subsequent manipulation.

In order to eliminate any effects of rotation or translation introduced by projection onto the tablet, the following transformations were applied (see Fig. 4):

$$x' = x_T - x_{A1}$$

$$y' = y_T - y_{A1}$$

$$x = (s' - y' \sin\alpha)\cos\alpha$$

$$y = y'/\cos\alpha + x\sin\alpha$$

where $\alpha = \tan^{-1}[(x_{A2} - x_{A1})/(y_{A2} - y_{A1})]$, and $A1$, $A2$ are calibration marks on the wind wall or bottom, as is appropriate. The data then were scaled to physical dimensions using the known distance between the recorded calibration marks.

Time Interpolation

Because the frame rates were different for the side and top cameras, digitized data were not time-synchronized on a frame-by-frame basis. In order to time synchronize the data, one of the sequences was interpolated linearly between frames. This provided two pairs of coordinate points in two essentially orthogonal views at the same time.

Three-Dimensional Reconstruction

The film as projected onto the digitizing tablet can be considered as a perspective transformation for each view; i.e., we have two two-dimensional views of the three-dimensional coordinates of the bubble. As pointed out by Sutherland,[5] the objective of the data reduction is to use the pairs of two-dimensional data points to determine the three-dimensional coordinate.

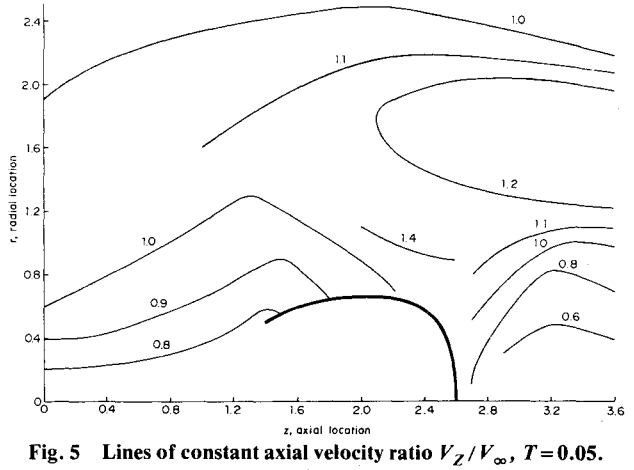

Fig. 5 Lines of constant axial velocity ratio V_Z/V_∞, $T=0.05$.

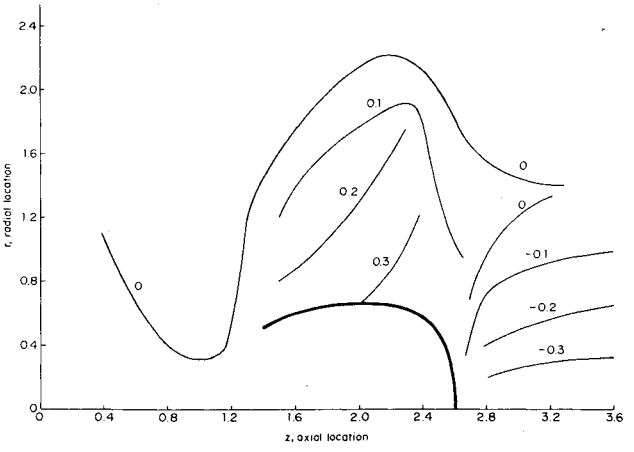

Fig. 6 Lines of constant radial velocity ratio V_r/V_∞, $T=0.05$.

In developing the data-reduction scheme, it is convenient to introduce homogeneous coordinates. In homogeneous coordinates, a point in three dimensions whose real coordinates are x, y, z is represented as a four-component row vector $[x\ y\ z\ 1]$ or as $[hX\ hY\ hZ\ h]$, where the homogeneous coordinate h is the fourth column in the row vector; h is completely arbitrary.

The general perspective transformation can be represented in homogeneous coordinates as a 4×4 transformation matrix, e.g.,

$$[x\ y\ z\ 1][T'] = [x'\ y'\ z'\ H]$$

where T' is a 4×4 transformation matrix:

$$T' = \begin{bmatrix} T_{11} & T_{12} & T_{13} & T_{14} \\ T_{21} & T_{22} & T_{23} & T_{24} \\ T_{31} & T_{32} & T_{33} & T_{34} \\ T_{41} & T_{42} & T_{43} & T_{44} \end{bmatrix}$$

This perspective transformation is a transformation from one three-dimensional space to another three-dimensional space. The results can be projected onto a two-dimensional plane, say the $z=0$ plane, by the transformation

$$T'' = \begin{bmatrix} 1 & 0 & 0 & 0 \\ 0 & 1 & 0 & 0 \\ 0 & 0 & 0 & 0 \\ 0 & 0 & 0 & 1 \end{bmatrix}$$

Concatenation of the two transformations yields

$$T = T'T'' = \begin{bmatrix} T_{11} & T_{12} & 0 & T_{14} \\ T_{21} & T_{22} & 0 & T_{24} \\ T_{31} & T_{32} & 0 & T_{34} \\ T_{41} & T_{42} & 0 & T_{44} \end{bmatrix}$$

The column of zeros shows that the matrix does not have an inverse. This is the mathematical statement of the well-known fact that it is not possible to reconstruct a three-dimensional object from a single-perspective projection. However, it is possible to reconstruct a three-dimensional position from two perspective views, say two photographs.

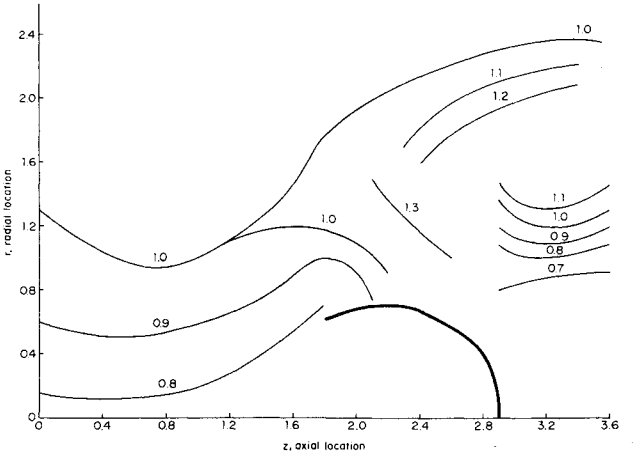

Fig. 7 Lines of constant axial velocity ratio V_Z/V_∞, $T=0.25$.

Let us write out the transformation, say,

$$[x\ y\ z\ 1]\begin{bmatrix} T_{11} & T_{12} & 0 & T_{14} \\ T_{21} & T_{22} & 0 & T_{24} \\ T_{31} & T_{32} & 0 & T_{34} \\ T_{41} & T_{42} & 0 & T_{44} \end{bmatrix} = [x'\ y'\ 0\ H] = H[u\ v\ 0\ 1]$$

where u, v are the ratios $u=x'/H$, $v=y'/H$, i.e., the coordinates in the perspective view, e.g., in the photograph. Writing out these equations yields

$$T_{11}x+T_{21}y+T_{31}z+T_{41}=Hu$$

$$T_{12}x+T_{22}y+T_{32}z+T_{42}=Hv$$

$$T_{14}x+T_{24}y+T_{34}z+T_{44}=H$$

Solving for H from the last equation and substituting yields

$$(T_{11}-T_{14}u)x+(T_{21}-T_{24}u)y$$
$$+(T_{31}-T_{34}u)z+(T_{41}-T_{44}u)=0$$
$$(T_{12}-T_{14}v)x+(T_{22}-T_{24}v)y$$
$$+(T_{32}-T_{34}v)z+(T_{42}-T_{44}v)=0$$

Assuming that the elements of the T transformation are known and that u and v are coordinates in the perspective projection, then with two views we may write four equations in the three unknowns x, y, z: the physical coordinates. The problem is, of course, overspecified, and x, y, z must be solved for in some "best-fit" sense. Writing the problem out in detail yields

$$(T^1_{11}-T^1_{14}u^1)x+(T^1_{21}-T^1_{24}u^1)y$$
$$+(T^1_{31}-T^1_{34}u^1)z+(T^1_{41}-T^1_{44}u^1)=0$$
$$(T^1_{12}-T^1_{14}v^1)x+(T^1_{22}-T^1_{24}v^1)y$$
$$+(T^1_{32}-T^1_{34}v^1)z+(T^1_{42}-T^1_{44}v^1)=0$$
$$(T^2_{11}-T^2_{14}u^2)x+(T^2_{21}-T^2_{24}u^2)y$$
$$+(T^2_{31}-T^2_{34}u^2)z+(T^2_{41}-T^2_{44}u^2)=0$$
$$(T^2_{12}-T^2_{14}v^2)x+(T^2_{22}-T^2_{24}v^2)y$$
$$+(T^2_{32}-T^2_{34}v^2)z+(T^2_{42}-T^2_{44}v^2)=0$$

where the superscripts correspond to views 1 and 2. This can be written in matrix form as

$$[A][X]=[B]$$

where

$$[A]=\begin{bmatrix} T^1_{11}-T^1_{14}u^1 & T^1_{21}-T^1_{24}u^1 & T^1_{31}-T^1_{34}u^1 \\ T^1_{12}-T^1_{14}v^1 & T^1_{22}-T^1_{24}v^1 & T^1_{32}-T^1_{34}v^1 \\ T^2_{11}-T^2_{14}u^2 & T^2_{21}-T^2_{24}u^2 & T^2_{31}-T^2_{34}u^2 \\ T^2_{12}-T^2_{14}v^2 & T^2_{22}-T^2_{24}v^2 & T^2_{32}-T^2_{34}v^2 \end{bmatrix}$$

$$[X]=\begin{bmatrix} x \\ y \\ z \end{bmatrix}$$

$$[B]^T=[T^1_{44}u^1-T^1_{41}T^1_{44}v^1-T^1_{42}T^2_{44}u^2-T^2_{41}T^2_{44}v^2-T^2_{42}]$$

A mean-squares fit can be computed by solving the equation

$$[A]^T[A][X]=[A]^T[B]$$

where $[A]^T$ is the transpose of $[A]$, and $[A][A]^T$ is square and of the right dimension to suit $[B]$. In particular,

$$[X]=\{[A^T][A]\}^{-1}[A]^T[B]$$

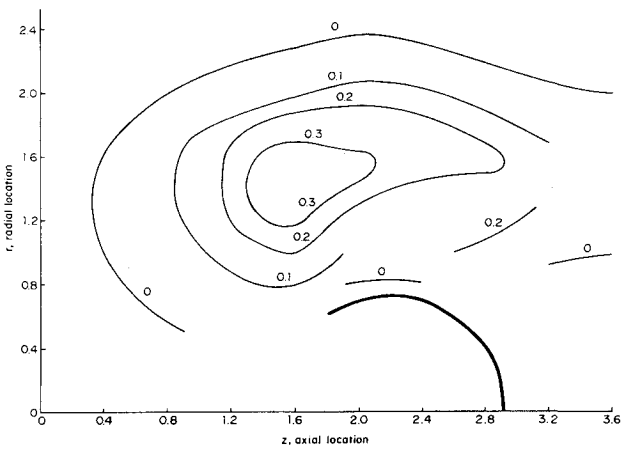

Fig. 8 Lines of constant radial velocity ratio V_r/V_∞, $T=0.25$.

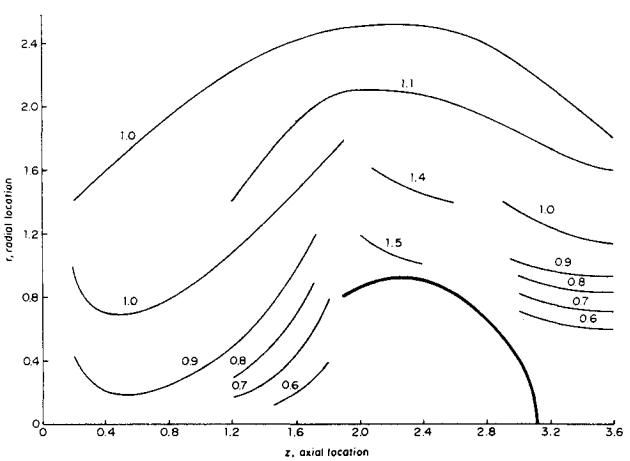

Fig. 9 Lines of constant axial velocity ratio V_Z/V_∞, $T=0.50$.

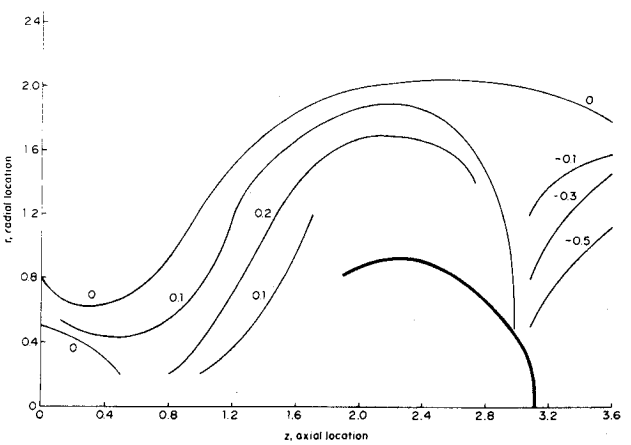

Fig. 10 Lines of constant radial velocity ratio V_r/V_∞, $T=0.50$.

If no solution results, then the imposed conditions are redundant, and no one solution represents the least-error condition.

Perspective Transformation

In order to utilize the data-reduction technique discussed previously, a knowledge of the transformations resulting from the use of the Fastax movie cameras is required. These transformations may, in general, be a combination of three-dimensional rotations, translations, and perspective projections. Using the results given in Ref. 6 and the tunnel-camera geometry, the transformations for the side and top camera views are

$$\begin{bmatrix} 0.999762 & 0 & 0 & 0 \\ -3.968631\times10^{-4} & 0.999835 & 0 & 0 \\ -2.181127\times10^{-2} & -1.81923\times10^{-2} & 0 & 4.863222\times10^{-3} \\ 0 & 0 & 0 & 1 \end{bmatrix}$$

and

$$\begin{bmatrix} 0.99848 & 0 & 0 & 0 \\ 1.5229\times10^{-4} & 0.999962 & 0 & 0 \\ 1.74517\times10^{-2} & -8.72654\times10^{-3} & 0 & 7.54717\times10^{-3} \\ 0 & 0 & 0 & 0 \end{bmatrix}$$

respectively.

In order to demonstrate the accuracy of the method just discussed for reconstructing three-dimensional information from two perspective views, these transformations were applied to the three-dimensional point [0.5 0.5 0.5] to obtain the projected points. For the side view, the results were [0.4875913 0.489713] and for the top view [0.506873 0.4937545]. The technique discussed previously then was used to reconstruct the three-dimensional coordinates. The result was [0.499997 0.50034 0.499546]. The accuracy of the method thus is established.

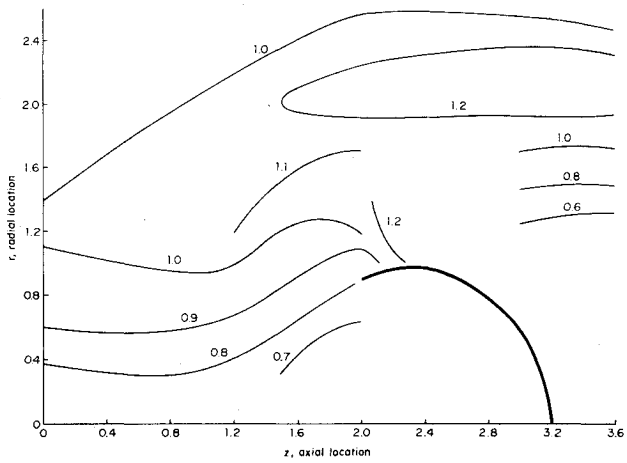

Fig. 11 Lines of constant axial velocity ratio V_Z/V_∞, $T=0.75$.

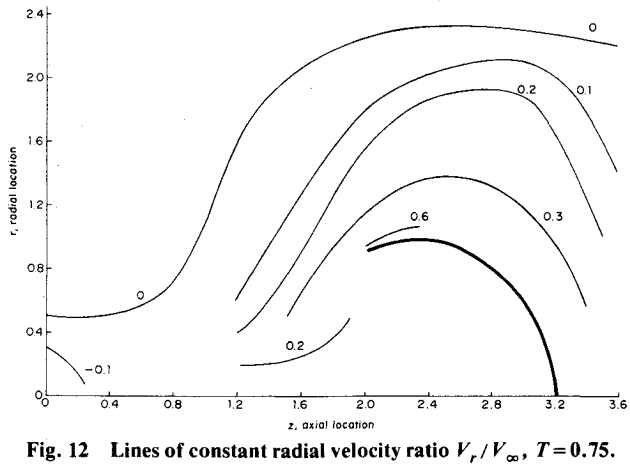

Fig. 12 Lines of constant radial velocity ratio V_r/V_∞, $T=0.75$.

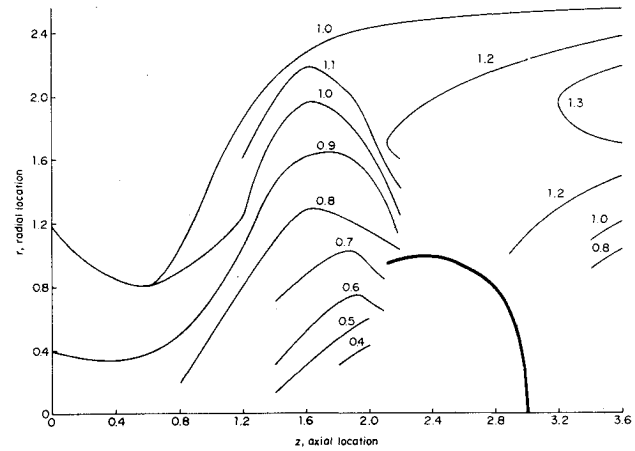

Fig. 13 Lines of constant axial velocity ratio V_Z/V_∞, $T=1.00$.

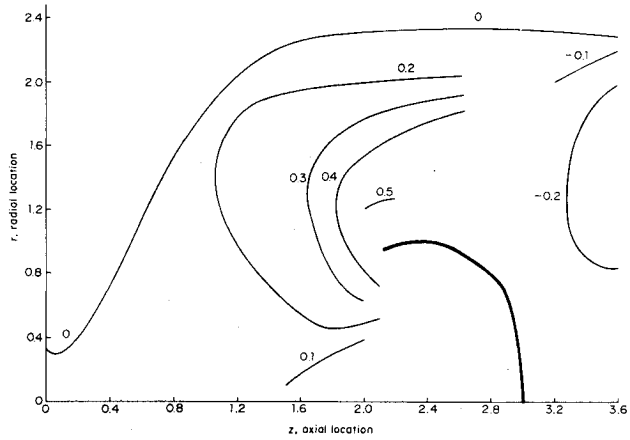

Fig. 14 Lines of constant radial velocity ratio V_r/V_∞, $T=1.00$.

Velocity Determination

The three-dimensional position vector obtained using the foregoing procedure was differentiated numerically as a function of time using a three-point central-difference formulation to obtain the Cartesian components of the velocity. These components then were combined to obtain the total velocity and appropriate polar components. The results then were nondimensionalized.

V. Results

In order to be succinct, velocity data are presented only for discrete times during the opening process. The filling time t_f was found for each of the 10 runs as the time when the maximum diameter (two-view average) was equal to 0.65 times the 18-in. nominal diameter.[7] These values ranged from 0.0165 to 0.0330 sec, with the mean at 0.0236 sec.§ Six time points were selected at which to present velocity information. These were $T=0.05$, 0.25, 0.50, 0.75, 1.0, and steady

§These filling times are considerably shorter than those predicted in Ref. 7, but the initial projected areas here were much greater than those of the cited study. When both projected area histories are examined as a function of actual time, the projected areas of both studies coincide over the portions of the opening which are common.

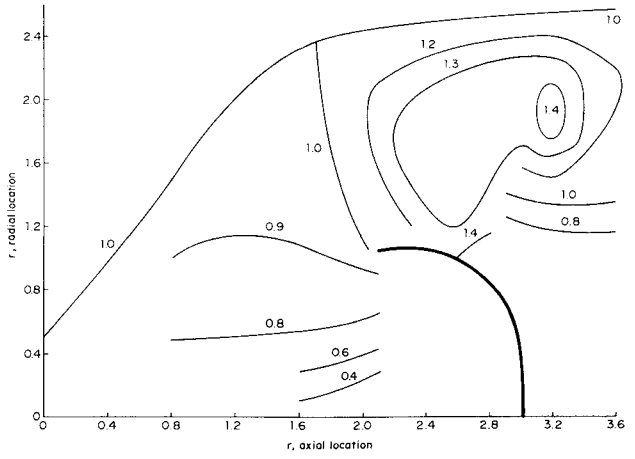

Fig. 15 Lines of constant axial velocity ratio V_Z/V_∞, $T=\infty$.

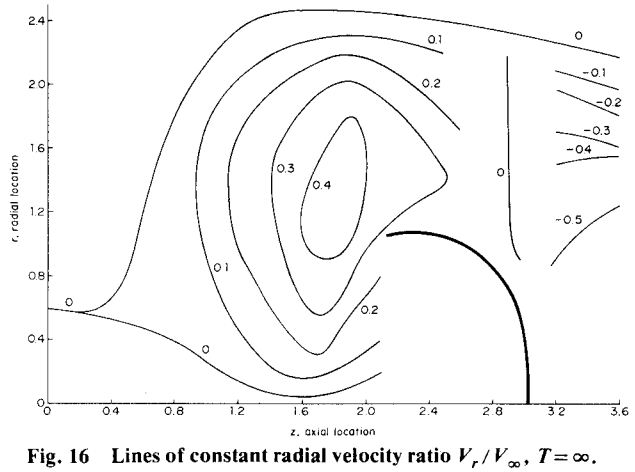

Fig. 16 Lines of constant radial velocity ratio V_r/V_∞, $T=\infty$.

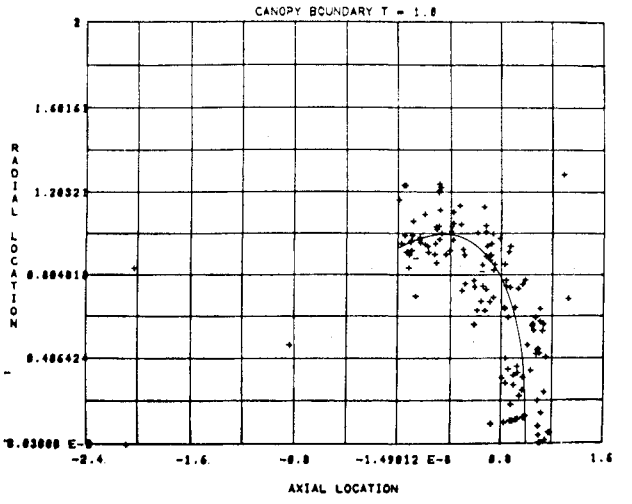

Fig. 17 Actual and mean canopy boundary locations, $T=1.0$.

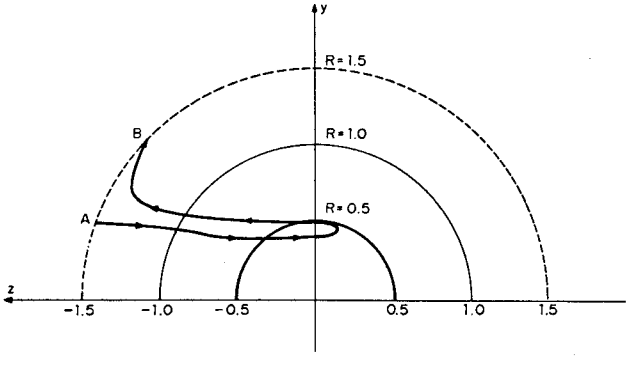

Fig. 18 Projection onto the y-z plane of a particle pathline downstream of canopy undergoing ring-vortex-type motion.

state ($T>1.75$). The flowfield velocities for these times were extracted from the full set from intervals ranging between $\pm 0.05T$ on either side of the nominal times. This interval width was needed to provide an adequate number of data points at each of the nominal times. The inflective nature of the maximum inflation portion of the sequence did not afford sufficient interval width to include a meaningful amount of information and was not examined. The axial coordinate was divided into 17 unequal intervals. These were about 1 in. near the canopy and considerably wider at the upstream and downstream extremities of the flowfield. The axial, radial, and circumferential position, then all were filed according to the time and axial location intervals into which they fell. Approximately two-thirds of the 3000 original bubble-frame pairs remained after this sort. An analysis of the circumferential velocities showed the average and rms values to be $-0.07\ V_\infty$ and $0.04\ V_\infty$, respectively. These low magnitudes appeared to be sufficient cause to assume axial symmetry, and all future references to circumferential location were dropped. First- and second-order least-square curves then were passed through the data in each file, and each of the axial and radial velocity components was plotted as a function of radial location. After the least-squares information was transferred to (r,z) plots for the time intervals of interest, velocity isolines were faired, resulting in Figs. 5-16. These smooth isolines agree between $\pm 0.1 V_\infty$ of the least-square curves. The canopy profiles shown in these figures are also 10-run composites. They were generated first by digitizing seven arbitrarily selected points along the actual canopy-projected boundary at five or six frame intervals in each of the side and top views. Figure 17 gives the canopy locations for the time interval $0.95 \le T \le 1.05$.

Where they may be compared to the results of Ref. 4 ($T=1.0$, ∞), the present velocity information is similar. Steady-state velocities were found for much greater portions of the mouth wake regions in the present work. This is primarily because of a pulsing or "breathing" of the canopy at the 100-fps airspeed, which did not appear in the 10-fps airspeed of Ref. 4. The actual canopy oscillated about the mean indicated in Figs. 15 and 16, and the accompanying variations in the flowfield included a sometimes smaller wake area and higher net velocity mouth region.

A number of bubbles in the wake region experienced motion characteristic of fluid near a ring vortex whose plan was parallel to that of the canopy mouth. Although not observed at the mouth, their initial detection in time and space was such that they well may be starting-type vortices shed from the skirt as the suspension lines began to retard the skirt's radial motion substantially. Figure 18 is a view of the pathline followed by one bubble apparently under the influence of a ring vortex. Projected onto the y-z plane and looking upstream, the motion under examination begins (point A) at an axial location of approximately 2.2 nominal radii downstream from the skirt and terminates (point B) at the same axial location. The axial excursion on the path between the two points reached a maximum of 2.9 radii and a minimum of 0.8 units. The time at which point A was reached by the bubble, $T=1.56$, is of some significance if it is assumed that the vortex also was near that axial location at that time. Projecting rearward in time at the freestream velocity rate of 100 fps, the ring would have been at the skirt at $T=1.14$. This is in the vicinity of canopy maximum projected diameter and lends support to the idea that the effects of a starting vortex are what are being sensed. Point B corresponds to $T=2.08$.

VI. Conclusions

High-speed motion-picture photography and a highly automated handling scheme have been combined with helium-filled soap-bubble generating apparatus to form a viable flow visualization system with the capability of providing quantitative velocity information. Although the low-airspeed opening of a flat circular parachute model was the subject of the present study, the techniques developed could be applied to a variety of low-speed, unsteady, or steady flow situations. Axial and radial velocities were measured for the airstream surrounding the canopy model from the time of suspension line extension into that of steady-state operation. Where comparison was possible, the velocities substantially agreed with those measured in an earlier study.

Acknowledgment

This work was supported by the U.S. Army Airdrop Engineering Laboratory, Natick, Mass.

References

[1] Heinrich, H. G., "Theory and Experiment on Parachute Opening Shock and Filling Time," *Royal Aeronautical Society Meeting*, London, England, Sept. 16, 1971.

[2] White, B. R., "Numerical Solutions to the Opening Dynamics of a Parachute," Dept. of Aerospace Engineering, Iowa State Univ., Ames, Iowa, 1973.

[3] Pounder, E., "Parachute Inflation Process Wind-Tunnel Study," Equipment Lab., Wright-Patterson Air Force Base, WADC TR 56-391, Sept. 1956, pp. 17-18.

[4] Klimas, P. C., "Helium Bubble Survey of an Opening Parachute Flowfield," *Journal of Aircraft*, Vol. 10, Sept. 1973, pp. 567-569.

[5] Sutherland, I. E., "Three Dimensional Data Input by Tablet," Office of Naval Research, Contract N0014-72-C-0346, 1973.

[6] Rogers, D. F. and Adams, J. A., *Mathematical Elements for Computer Graphics*, McGraw-Hill, New York, 1976.

[7] Heinrich, H. G., "The Opening Time of Parachutes Under Infinite Mass Conditions," Summer Course on Aerodynamics Deceleration, Univ. of Minnesota, 1969.